RESEARCH PAPER

Synthesis and Structural Investigation of Erbium-Doped $ZnWO_4$ Nanocrystals

Forough Zunia [1], Morteza Raeisi [1]*, Sanaz Alamdari [2], Nooshin Heydarian Dehkordi [2]

[1] Physics department Faculty of Basic Science Shahrekord University, Shahrekord, Iran
[2] Department of Nanotechnology, Faculty of New Science and Technologies, Semnan University, Semnan, Iran

ARTICLE INFO

Article History:
Received 01 Aug 2023
Accepted 05 Dec 2023
Published 01 Jan 2024

Keywords:
$ZnWO_4$,
Er dopant,
Co-precipitation,
Morphology,
Strain.

ABSTRACT

In this study, $ZnWO_4$:Er^{3+} nanocrystals were synthesized using a simple co-precipitation method. The structural properties of the prepared powders were characterized through X-ray diffraction (XRD), Fourier-transform infrared spectroscopy (FTIR), and field emission scanning electron microscopy (FE-SEM). The synthesized nanopowders exhibited a monoclinic wolframite crystal structure. Using the Williamson-Hall method, the lattice strain and crystal size of the synthesized powders were estimated. ZWO nanopowders with a 1 at.% concentration of Er dopant showed the lowest strain and crystallite size. FE-SEM results revealed that the prepared nanoparticles have a spherical morphology with an average size of 140 nm. The FTIR analysis confirmed the presence of Zn-O, Zn-O-W, and W-O vibrations in the synthesized structure. The transmittance percentage in the doped sample changed concerning the pure one, indicating that interstitial Er3+ ions affected the number of W-O, Zn-O, and Zn-O-W bonds. The facilely synthesized Erbium-doped ZnWO4 nanocrystals showed promise for a range of practical applications.

How to cite this article
Zunia F., Raeisi M., Alamdari S., Heydarian Dehkordi N., Synthesis and Structural Investigation of Erbium-Doped ZnWO4 Nanocrystals. Nanochem. Res., 2024; 9(1): 28-34. DOI: 10.22036/NCR.2024.01.04

INTRODUCTION

Zinc tungstate ($ZnWO_4$ or ZWO) is one of the most applicable divalent-transition metal tungstates with monoclinic wolframite structure and P2/c space group [1]. The ZWO structure consists of zigzag chains of distorted ZnO_6 and WO_6 octahedra composed of two groups of oxygen atoms (O_1 and O_2). Each octahedron (ZnO_6 and WO_6) shares its two corners with the adjacent octahedron (each of the ZnO_6 or WO_6 octahedra). The ZnO_6 octahedron comprises of four O_2 and two O_1, while the WO_6 octahedron consists of two O_2 and four O_1 atoms. Zn-O_1, W-O_1, Zn-O_2, and W-O_2 bond lengths are 0.20 nm, 0.19 nm, 0.22 nm, and 0.18 nm, respectively. O_2-Zn-O_1, O_2-W-O_1, O_1-Zn-O_1, O_1-W-O_1, O_2-Zn-O_2, and O_2-W-O_2 bond lengths are 94.82 nm, 89.29 nm, 106.35 nm, 79.41 nm, 76.32, and 102.94 nm, respectively [1, 2]. (The schematic diagram of the ZWO unit cell is shown in Fig. 1.)

ZWO, a self-activating phosphor, emits a broad blue-green light under deep UV excitation [1-4]. It possesses high refractive index, thermal and chemical stability, short decay time, non-toxicity, and high light yield. Due to these features, ZWO finds applications in optical devices, displays, scintillators, photoanodes, laser hosts, optical fibers, humidity sensors, microwave devices, photoluminescence, photovoltaics, photonics, and tomography [1-6]. Its monoclinic wolframite structure makes it a promising up-conversion host for lanthanides. Various synthesis methods, such as chemical precipitation, solid-state reaction, spray pyrolysis, co-precipitation, solvothermal, and sol-gel, enable the quick preparation of ZWO

* Corresponding Author Email: raeisi.morteza@gmail.com

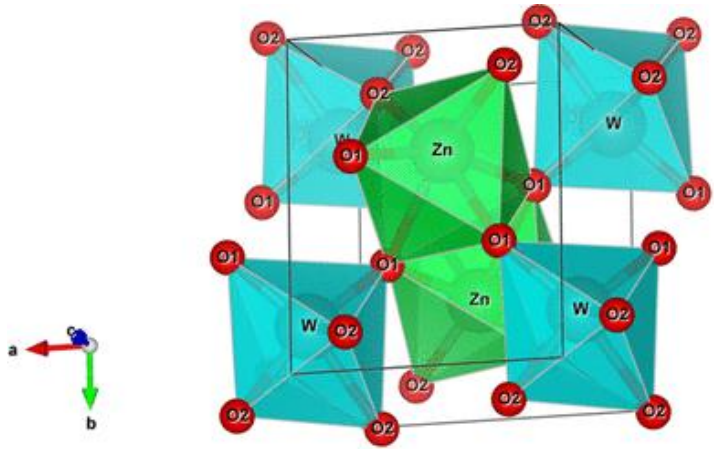

Fig. 1. The schematic diagram of the ZWO unit cell [2].

nanoparticles. Incorporating trivalent rare-earth ions, such as Er^{3+}, enhance luminescence in the visible region. Er^{3+} doping in ZWO has been explored for temperature sensing, with potential applications in bioimaging [6-8]. Srivastava et al. synthesized $ZnGa_2O_4$:Yb^{3+}, Er^{3+}, and Cr^{3+} (ZGO-YEC) NPs that emit a bright single red emission under 980 nm excitation [9]. Biswas et al. incorporated Er^{3+}-Yb^{3+}-Na^{+} into ZWO, improving up-conversion and temperature sensing [10]. It was reported that synthesized Y2O3: Yb^{3+}, Er^{3+} NPs demonstrated novel luminescence properties for bioimaging applications [10,11]. Although numerous studies have investigated the optical properties of pure/doped tungstate families and dual mixed oxide compounds [3-15], the structure of ZWO: xEr^{3+} has received less attention. As mentioned above, the unique structural, dielectric, and optical properties of zinc tungstate ($ZnWO_4$) have garnered significant attention in recent years [1-6]. This compound, with its intriguing characteristics, holds promise for diverse applications in various fields. Research on $ZnWO_4$ has been extended to explore its potential use in fields such as optoelectronics, photocatalysis, and photonic applications [2]. Understanding the structural intricacies, dielectric behavior, and optical features of $ZnWO_4$ is essential for harnessing its full potential. Recent studies have delved into the comprehensive analysis of ZnWO4's properties. For instance, Dkhilalli et al. conducted a thorough investigation into the structural, dielectric, and optical properties of $ZnWO_4$, shedding light on its potential applications [2]. Additionally, the work of Xueyan Liu et al. (2023) introduced a novel p-n heterojunction photocatalyst involving $CoWO_4/ZnWO_4$, showcasing the compound's versatility in enhancing photocatalytic activity under visible light irradiation [4]. Moreover, the research by Rafael W.R. Santana et al. (2023) explored the development of BiOBr/$ZnWO_4$ heterostructures for enhanced photocatalytic degradation, highlighting the compound's potential in environmental remediation [3]. These recent investigations underscore the growing interest in $ZnWO_4$ and its multifaceted applications, paving the way for further exploration and utilization of this intriguing material. In this study, ZWO: Er^{3+} NPs were prepared using a simple method, and their structure was investigated for our future optical properties report.

EXPERIMENTAL SECTION

Synthesis of Nanoparticles

Pure ZWO and ZWO: Er^{3+} NPs were synthesized using a co-precipitation method followed by calcination. Initially, a solution was prepared by dissolving zinc acetate and sodium tungstate in 50 cc of deionized water. Subsequently, the tungstate solution was gradually introduced into the zinc solution. In the subsequent step, approximately 2 hours later, concentrations of 0.5 and 1at. % Er $(NO_3)_3.6H_2O$ were mixed with 10 ccs of deionized water and added drop by drop to the aforementioned solution. The resulting mixture was subjected to centrifugation and subsequently dried at a temperature of 80 ℃ for a duration of 24 hours. Finally, the obtained powder was subjected to calcination at a temperature of 600 ℃ for a period of 2 hours. Erbium ions typically replace some of the zinc (Zn) ions in the crystal lattice. Erbium is commonly used as a dopant in various

materials to introduce luminescent properties, and it can substitute for metal cations like Zn^{2+} or other cations in the host crystal lattice. Thus, in the case of $ZnWO_4$ with erbium doping, erbium ions are likely to replace zinc ions in the crystal structure. This substitution allows erbium to introduce its unique optical properties into the material, making it suitable for various applications in optics and photonics.

Characterization

The crystallinity, phase, and crystal structure of the powders were examined using a Bruker D8 X-ray powder diffractometer, operating with Cu Kα radiation (λ = 0.15406 nm) collected at 10°≤2θ≤70°. Fourier transform infrared spectroscopy (FTIR, Perkin Elmer RX) was employed to recognize the bending and stretching vibrations of Zn-O, Zn-O-W, and W-O bonds. Field-emission scanning electron microscopy (FE-SEM, MIRA III TESCAN) revealed the morphology and size distribution of NPs.

RESULTS AND DISCUSSION

Crystal Structure

The XRD patterns of the as-synthesized ZWO and ZWO: Er^{3+} phosphors and the JCPDS standard pattern (reference number 01-088-0251) presented in Fig. 2 indicated that the main phase of the powders was $ZnWO_4$ (JCPDS: 01-088-0251) with a monoclinic wolframite structure and space group P2/c. The XRD pattern of ZWO and ZWO: 1 at. % Er^{3+} nanopowders exhibited additional peaks marked with circles attributed to the low number of tungsten oxides [15]. A comparison between the two main diffraction peaks of ZWO (-111) and (111) in ZWO: x Er^{3+} (x=0, 0.5, and 1 at. %) was obtained (Fig. 1b), which demonstrates that the main peaks in doped samples, particularly in the state of x=1%at. The shift toward larger angles is attributed to the substitution of $3Zn^{2+}$ ions with $2Er^{3+}$ ions in the host lattice and the creation of a Zn^{2+} vacancy (V_{Zn}^{2+}), which has caused the contraction of the crystal lattice, and then a reduction in the distance between the planes of the lattice. The intensity of the main diffraction peaks decreased in the doped samples, especially at x=0.5 at. %, indicating a decrease in crystallinity. The number of defects, such as V_{Zn}^{2+}, interstitial O^{2-} vacancies, or other trapping defects in the crystal lattice of ZWO: 0.5 at. % Er was higher than that of the ZWO: 1 at. % Er^{3+}, leading to disorder in the local symmetries around the radiative centers and a reduction in crystallinity.

Using Williamson-Hall's method and XRD data, the crystal size and lattice strain values of NPs were calculated, as shown in Fig. 3. According to the Williamson-Hall results, the crystal sizes in ZWO, ZWO: Er (0.5 at. %), ZWO: Er (1 at. %), were 55 nm, 30 nm, and 45.2 nm, respectively. The crystal size in the doped samples and especially the ZWO: Er (0.5 at. %) diminished while the strain increased, indicating that Zn^{2+} ions were substituted well with Er^{3+} ions.

FTIR spectroscopy

Fig. 3 illustrates the FTIR spectra of the as-synthesized powders. The spectra confirmed the formation of zinc tungstate from the appearance of vibrational bands related to Zn-O, W-O, stretching, and symmetric vibrations of bridging oxygen atoms of Zn-O-W groups. As shown in Fig. 4, eight

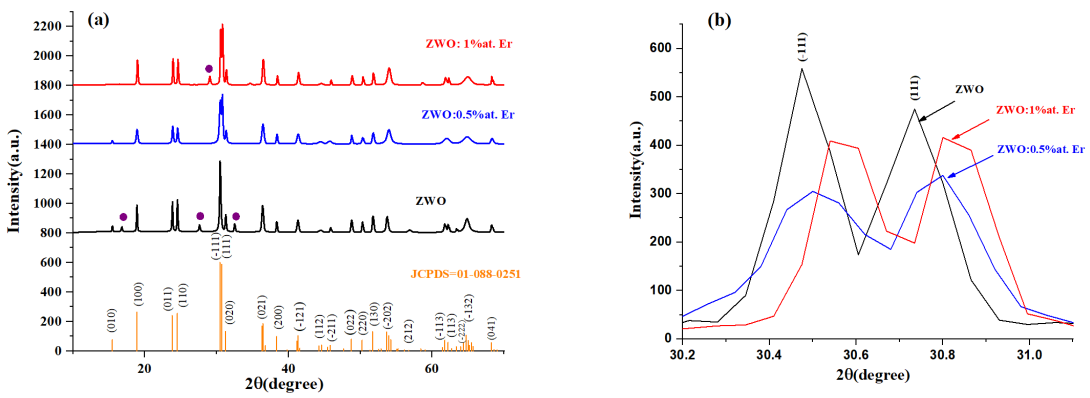

Fig. 2. (a). XRD patterns of ZWO, ZWO: 0.5% at. Er^{3+}, ZWO: 1% at. Er^{3+} nanopowders and reference data for ZWO (JCPDS: 01-088-251) (b). Comparison between (111) and (-111) diffraction peaks.

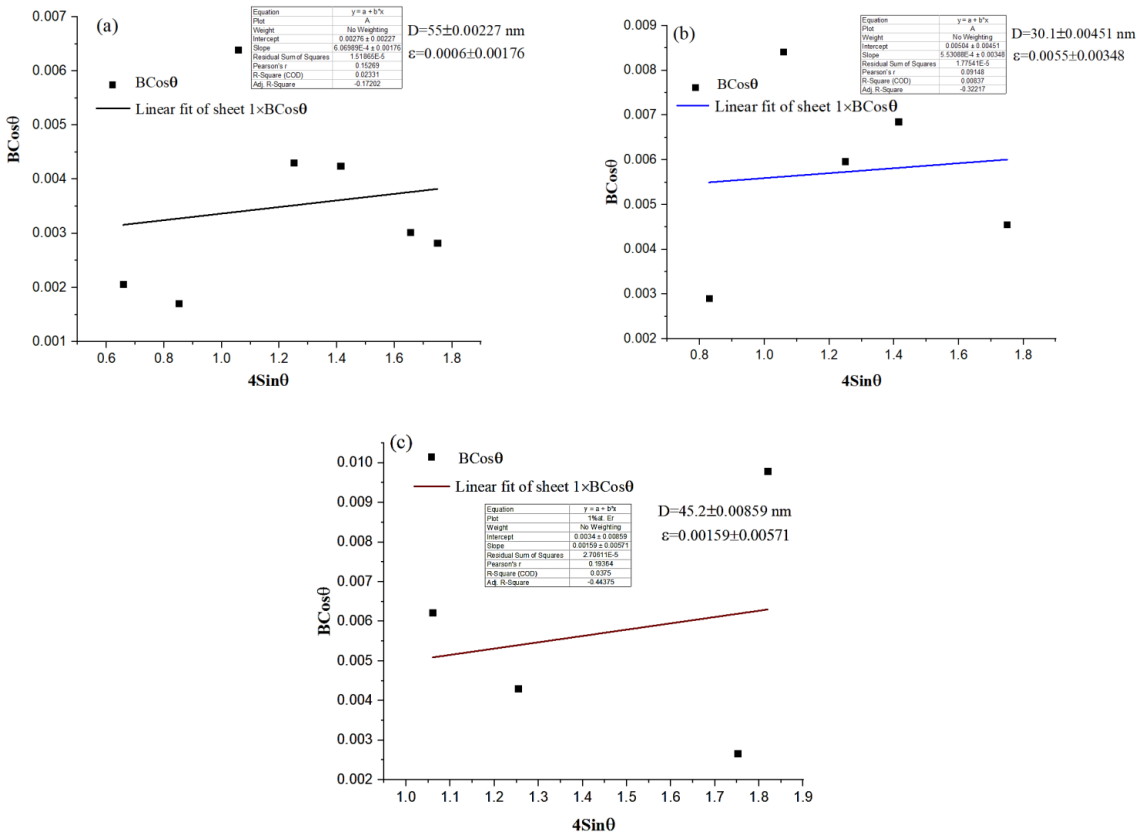

Fig.. 3. Williamson-Hall plot (BCosθ - 4Sinθ) for (a) ZWO, (b) ZWO: 0.5%at. Er^{3+} and (c) ZWO: 1at. % Er^{3+} nanopowders.

vibration modes in the fingerprint region of the infrared spectrum (1600-400 cm-1) are related to the W-O and Zn-O vibrations. The bands observed at 428.2 cm^{-1} and 472 cm^{-1} are attributed to the band and stretching vibrations of Zn-O, respectively. This attribution is consistent with previous articles (432 and 473 cm^{-1}) [16, 17].

The 3 bands at 532.32, 697, and 716 cm^{-1} are due to the symmetric and asymmetric stretching vibrations of bridging atoms in WO_2 groups of distorted octahedra WO_6^{-6}, which are consistent with other studies [18, 19]. The bands at 532.32 and 716 cm^{-1} correspond to the symmetric vibrations of the bridging oxygen atoms in the Zn-O-W group [20]. The symmetric vibrations of the bridging oxygen atoms of Zn-O-W groups produce broad absorption bands at 833.19 and 873 cm^{-1} [18]. The vibrational modes at 1633.59 and 3460.06 cm^{-1} correspond to the bending and stretching vibrations of the OH group reported to locate at 1644 and 3448 cm^{-1}, respectively [19, 21]. The results align with those of previous studies [22-26]. According to Fig. 3b, the transmission in the near-infrared region (NIR) increased in doped samples, especially in ZWO:1 at. % Er sample. It is expected that the pure ZWO will have better structural and optical characteristics due to having less transmission and more bonds in that frequency region. In the pure sample, the degree of crystallinity was higher, the bonds were complete, and a more complete structure was formed. ZWO:1 at. % Er transmittance percentage increased in 428-873 cm^{-1}, while it decreased in ZWO:0.5 at. % Er sample. The number of Zn-O-W and W-O bonds in ZWO: 1 at. % Er sample decreased, indicating the interstitial Er atoms in the ZWO structure, while the number of Zn-O-W and W-O bonds elevated in ZWO: 0.5 at. % Er. No significant displacements appeared in the location of the transmittance bands of samples.

Morphology

Fig. 5 displays the FE-SEM images, size distribution, and EDAX-map of the ZWO: Er^{3+} NPs prepared by the co-precipitation method. As shown in Fig. 5, the crystals in the ZWO: 1at. % Er^{3+}

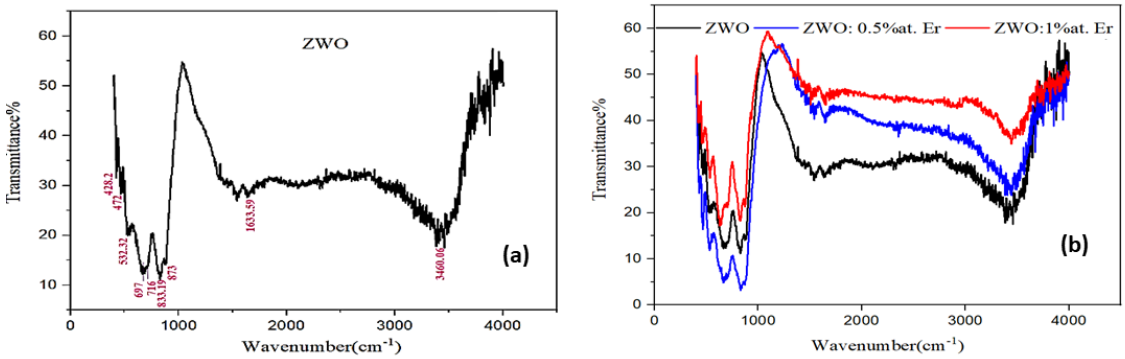

Fig. 4. FTIR spectra of ZWO, ZWO: 0.5%at. Er, and ZWO: 1%at. Er powders.

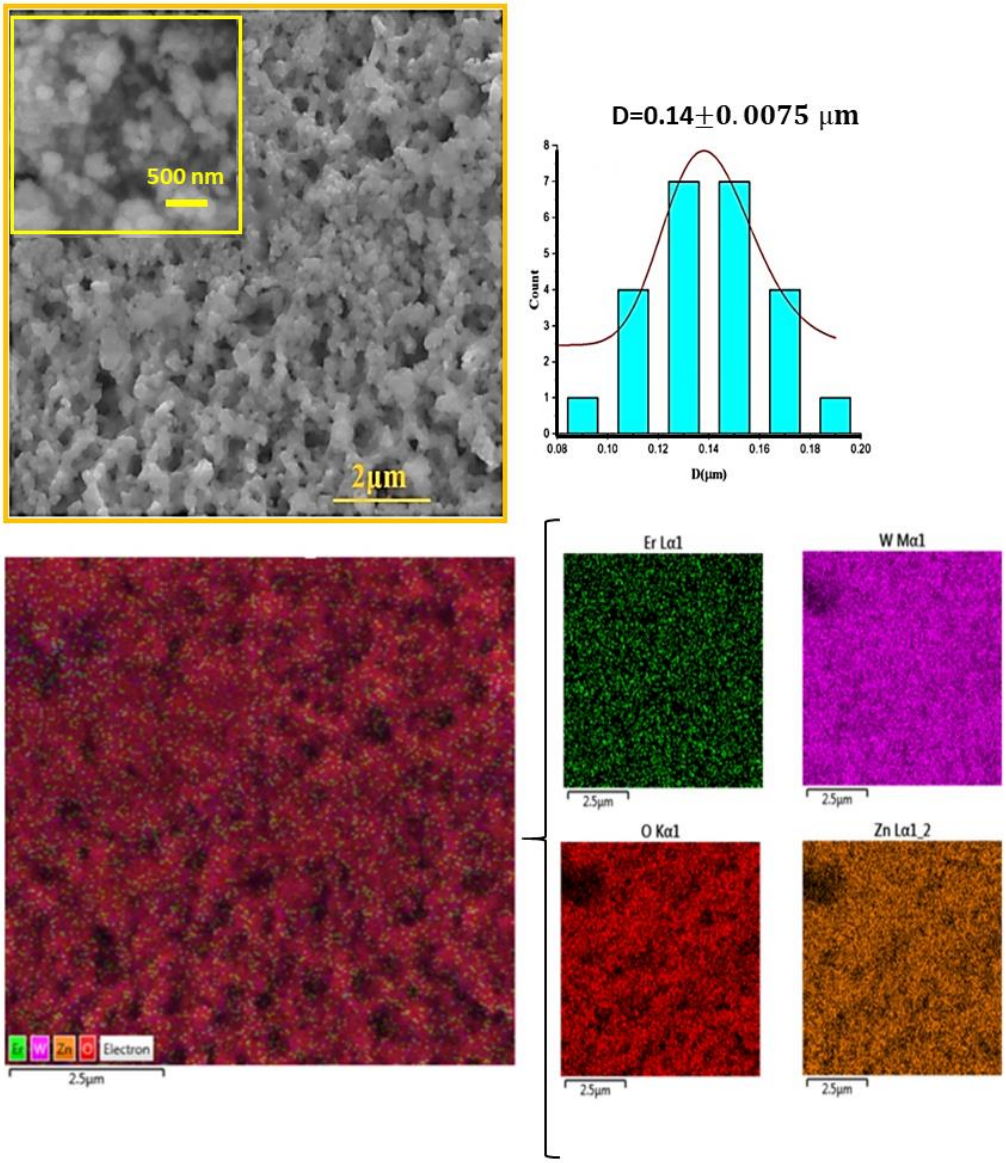

Fig. 5. FE-SEM image, particle size distribution, and EDS-map of ZWO: 1 at. % Er^{3+} powder.

sample have a spherical morphology agglomerated in some parts with an average size of 140 nm. According to the EDS-map images, the distribution of Er, Zn, W, and O atoms was uniform.

CONCLUSION

In this article, pure and Er doped ZWO nanocrystals were prepared by using nanoscience and eco-friendly materials. The XRD results demonstrated that the samples had a monoclinic wolframite structure. The diffraction pattern of the ZWO: 0.5 at. % Er^{3+} was without an additional peak (related to tungsten oxide). The crystallinity of the pure sample was higher than that of the doped samples. Williamson-Hall's results demonstrated that the size of the crystals in the ZWO: 0.5 at. % Er^{3+} sample decreased up to 30 nm and, the Er^{3+} ions replaced the Zn^{2+} ions in the ZWO lattice. SEM images revealed that nanoparticles agglomerated exhibited spherical morphology and an average size of 140 nm. The transmittance percentage in the doped sample changed concerning the pure one, indicating that interstitial Er^{3+} ions affected the number of W-O, Zn-O, and Zn-O-W bonds. The products have the potential for the production of flexible detectors and green lasers in future.

CONFLICT OF INTEREST

The authors declare no conflicts of interest.

REFERENCES

1. Azadmehr S, Jafat Taftreshi M, Alamdari S. Synthesis, Characterization and Scintillation Response of ZnWO4-GO Nanocomposite. Journal of Composites and Compounds. 2022;4(12):158-62. https://doi.org/10.52547/jcc.4.3.5
2. Dkhilalli F, Borchani SM, Rasheed M, Barille R, Guidara K, Megdiche M. Structural, dielectric, and optical properties of the zinc tungstate ZnWO4 compound. Journal of Materials Science: Materials in Electronics. 2018;29(8):6297-307. https://doi.org/10.1007/s10854-018-8609-z
3. Santana RWR, Lima AEB, Souza LKCd, Santos ECS, Santos CC, Menezes ASd, et al. BiOBr/ZnWO4 heterostructures: An important key player for enhanced photocatalytic degradation of rhodamine B dye and antibiotic ciprofloxacin. Journal of Physics and Chemistry of Solids. 2023;173:111093. https://doi.org/10.1016/j.jpcs.2022.111093
4. Liu X, Shu J, Wang H, Jiang Z, Xu L, Liu C. One-pot preparation of a novel CoWO4/ZnWO4p-n heterojunction photocatalyst for enhanced photocatalytic activity under visible light irradiation. Journal of Physics and Chemistry of Solids. 2023;172:111061. https://doi.org/10.1016/j.jpcs.2022.111061
5. Hemmati M, Tafreshi MJ, Ehsani MH, Alamdari S. Highly sensitive and wide-range flexible sensor based on hybrid BaWO4@CS nanocomposite. Ceramics International. 2022;48(18):26508-18. https://doi.org/10.1016/j.ceramint.2022.05.347
6. Hosseinpour M, Abdoos H, Mirzaee O, Alamdari S. Fabrication and characterization of a new flexible ionizing ray sensor based on lead tungstate (PbWO4). Ceramics International. 2023;49(3):4722-32. https://doi.org/10.1016/j.ceramint.2022.09.362
7. Hosseinpour M, Mirzaee O, Alamdari S, Menéndez JL, Abdoos H. Development of a novel flexible thin PWO(Er)/ZnO(Ag) nanocomposite for ionizing radiation sensing. Journal of Alloys and Compounds. 2023;967:171678. https://doi.org/10.1016/j.jallcom.2023.171678
8. Rabizadeh M, Ehsani MH. Effect of heat treatment on optical, electrical and thermal properties of ZnO/Cu/ZnO thin films for energy-saving application. Ceramics International. 2022;48(11):16108-13. https://doi.org/10.1016/j.ceramint.2022.02.158
9. Srivastava BB, Gupta SK, Mao Y. Single red emission from upconverting ZnGa2O4: Yb, Er nanoparticles co-doped by Cr 3+. Journal of Materials Chemistry C. 2020;8(19):6370-9. https://doi.org/10.1039/D0TC00411A
10. Biswas S, Mukhopadhyay L, Mondal M, Rai VK. Er3+-Yb3+-Na+:ZnWO4 phosphors for enhanced visible upconversion and temperature sensing applications. Journal of Rare Earths. 2021;39(3):291-6. https://doi.org/10.1016/j.jre.2020.02.018
11. Kamimura M, Miyamoto D, Saito Y, Soga K, Nagasaki Y. Preparation of PEG and protein co-immobilized upconversion nanophosphors as near-infrared biolabeling materials. Journal of Photopolymer Science Technology. 2008;21(2):183-7. https://doi.org/10.2494/photopolymer.21.183
12. Kamimura M, Kanayama N, Tokuzen K, Soga K, Nagasaki Y. Near-infrared (1550 nm) in vivo bioimaging based on rare-earth doped ceramic nanophosphors modified with PEG-b-poly(4-vinylbenzylphosphonate). Nanoscale. 2011;3(9):3705-13. https://doi.org/10.1039/c1nr10466g
13. He HY. Preparation and luminescence property of Sm-doped ZnWO4 powders and films with wet chemical methods. physica status solidi (b). 2009;246(1):177-82. https://doi.org/10.1002/pssb.200844218
14. Aliannezhadi M, Minbashi M, Tuchin VV. Effect of laser intensity and exposure time on photothermal therapy with nanoparticles heated by a 793-nm diode laser and tissue optical clearing. Quantum Electronics. 2018;48(6):559. https://doi.org/10.1070/QEL16505
15. Alamdari S, Ghamsari MS, Afarideh H, Mohammadi A, Geranmayeh S, Tafreshi MJ, et al. Preparation and characterization of GO-ZnO nanocomposite for UV detection application. Optical Materials. 2019;92:243-50. https://doi.org/10.1016/j.optmat.2019.04.041
16. Wang L, Ma Y, Jiang H, Wang Q, Ren C, Kong X, et al. Luminescence properties of nano and bulk ZnWO4 and their charge transfer transitions. Journal of Materials Chemistry C. 2014;2(23):4651-8. https://doi.org/10.1039/c4tc00245h
17. Huang G, Shi R, Zhu Y. Photocatalytic activity and photoelectric performance enhancement for ZnWO4 by fluorine substitution. Journal of Molecular Catalysis A: Chemical. 2011;348(1):100-5. https://doi.org/10.1016/j.molcata.2011.08.013
18. Siriwong P, Thongtem T, Phuruangrat A, Thongtem

S. Hydrothermal synthesis, characterization, and optical properties of wolframite ZnWO4 nanorods. CrystEngComm. 2011;13(5):1564-9. https://doi.org/10.1039/C0CE00402B

19. Pavithra NS, Nagaraju G, Patil SB. Ionic liquid-assisted hydrothermal synthesis of ZnWO4 nanoparticles used for photocatalytic applications. Ionics. 2021;27(8):3533-41. https://doi.org/10.1007/s11581-021-04123-9
20. Alharthi FA, Al-Nafaei WS, Alshayiqi AA, Alanazi HS, Hasan I. Hydrothermal Synthesis of Bimetallic (Zn, Co) Co-Doped Tungstate Nanocomposite with Direct Z-Scheme for Enhanced Photodegradation of Xylenol Orange. Catalysts [Internet]. 2023; 13(2). https://doi.org/10.3390/catal13020404
21. Zou H-Y, Wang X-G. Preparation and luminescence properties of ZnWO4:Eu3+,Tb3+ phosphors. Luminescence. 2021;36(6):1452-8. https://doi.org/10.1002/bio.4086
22. Irfan A, Al-Sehemi AG, Assiri MA, Mumtaz MW. Exploring the electronic, optical and charge transfer properties of acene-based organic semiconductor materials. Bulletin of Materials Science. 2019;42(4):145. https://doi.org/10.1007/s12034-019-1838-9
23. Wang X, Fan Z, Yu H, Zhang H, Wang J. Characterization of ZnWO4 Raman crystal. Opt Mater Express. 2017;7(6):1732-44. https://doi.org/10.1364/OME.7.001732
24. Salimi K, Eghbali S, Jasemi A, Shokrani Foroushani R, Joneidi Yekta H, Latifi M, et al. An Artificial Soft Tissue Made of Nano-Alginate Polymer Using Bioxfab 3D Bioprinter for Treatment of Injuries. Nanochemistry Research. 2020;5(2):120-7.
25. Madani M, Mansourian M, Alamdari S, Mirzaee O, Jafar Tafreshi M. Facile Synthesis and Characterization of Highly Luminescent Bi2WO6 Nanoparticles for Photonic Application. Nanochemistry Research. 2022;7(1):15-21.
26. Alamdari S, Majles Ara MH, Jafar Tafreshi M. Synthesize and optical response of ZnO/CdWO4: Ce nanocomposite with high sensitivity detection of ionizing radiations. Optics & Laser Technology. 2022;151:107990. https://doi.org/10.1016/j.optlastec.2022.107990